TECHNICAL REPORT STANDARD TITLE PAGE

1. Report No.	2. Gov. Acession No.	3. Recipient's Catalog No.
4. Title and Subtitle "In Situ Spectroradiometric Quantification of ERTS Data"		5. Report Date December 1972 6. Performing Organization Code
7. Author(s) Edward F. Yost		8. Performing Organization Report No. TR-21-I
9. Performing Organization Name & Address Science Engineering Research Group C.W. Post Center Long Island University Greenvale, New York 11548		10. Work Unit No. 11. Contract or Grant No. NAS5-21793
12. Sponsoring Agency Name & Address Mr. Edmund F. Szajna Goddard Space Flight Center Greenbelt, Maryland 20771		13. Type of Report and Period Covered Type II - July-December 1972 14. Sponsoring Agency Code

15. Supplementary Notes

16. Abstract

Additive color photographic analysis of ERTS-1 multispectral imagery indicates that the presence of soil moisture in Playas (desert dry lakes) can be readily detected from space. Time sequence additive color presentations in which 600-700 nm bands taken at three successive 18-day cycles show that changes in soil moisture of Playas with time can be detected as unique color signatures and can probably be quantitatively measured using photographic images of multispectral scanner data.

COLOR ILLUSTRATIONS REPRODUCED IN BLACK AND WHITE

17. Key Words (Selected by Author(s))	18. Distribution Statement
Spectroradiometric Quantification of Data	

19. Sec. Classif. (of this report)	20. Sec. Classif. (of this page)	21. No. of Pages	22. Price*
U	U	45	4.50

*For sale by the Clearinghouse for Federal Scientific and Technical Information, Springfield, Virginia 22151.

Table of Contents

Preface

The task of correlating in situ spectral reflectance measurements with ERTS imagery has commenced. A method of additive color analysis of a single multispectral band taken on different dates indicates that ERTS-1 bulk images have sufficient spatial and spectral fidelity to show indications of the presence of soil moisture in desert playas and changes in soil moisture with time. The chain of causality between soil moisture, in situ spectral reflectance, and ERTS multispectral scanner image density remains to be established during the subsequent phases of this study.

Section 1

Introduction

This report has been prepared in regard to NASA Contract NAS5-21793 for "In Situ Spectroradiometric Quantification of ERTS Data". This interim progress report covers the initial preparation, field work, analysis of imagery, and in situ reflectance spectra for the period July through December 31, 1972.

This project was undertaken by Long Island University to establish the relationship between in situ spectral reflectance measurements and the photometric characteristics of ERTS-1 multispectral scanner imagery. All imagery of the test site at Willcox Playa, Arizona, which was received was cloud free; however, clouds obscured a test site at Prescott National Forest, Arizona, where in situ spectral reflectance measurements were being obtained during the 27 September-2 November 1972 period of ERTS-1 image acquisition.

A "first look" analysis of the imagery was performed using a multispectral color viewer. The additive color analysis revealed the existence of significant spectral reflectivity differences in the Willcox Playa between 27 September and 2 November 1972. A time sequence analysis of the 600-700 nm (red) band was performed for the ERTS-1 acquisition dates of 27 September, 14 October, and 2 November 1972. This method of time sequence analysis permitted the association of differences in soil moisture over time with the color of the multispectral display. ERTS-1 bulk images were found of sufficient spatial fidelity to allow good image registration of the image of the Willcox Playa.

Incident and reflectance spectroradiometric measurements of the Willcox Playa obtained prior to the launch of ERTS-A have been computer processed for subsequent correlation with the imagery. In situ spectral reflectance measurements obtained of a test site in the Prescott National Forest, Arizona, during the period of ERTS-1 data collection have also been computer processed for correlation with multispectral data when cloud-free imagery is obtained.

Section 2

Analysis of ERTS-1 Imagery and Associated Spectroradiometric Ground Data

An analysis of the photographic characteristics of three sets of ERTS-1 data acquired over Willcox, Arizona, on 27 September, 14 October, and 2 November 1972 and a color analysis using additive color reconstruction of the imagery showed significant changes in the reflectance of the Willcox Playa during these dates. A time lapse multispectral technique was developed to enhance the color description of reflectance differences in a single band over time and is described in Section 2.2.

Relative spectral reflectance measurements of the Willcox Playa obtained prior to ERTS-1 launch have been computer processed for subsequent analysis. Reflectance spectra were obtained of predominant vegetation in the Prescott National Forest; however, cloud cover at the time of acquisition of ERTS-1 imagery precluded correlation of reflectance spectra with the imagery. The instrumentation used to acquire the spectra and the results obtained are described in Sections 2.3 and 2.4.

2.1 Additive Color Analysis of ERTS-1 Imagery of the Willcox Playa

The first set of scanner data which was analyzed was taken on 27 September 1972. Initially, a set of curves showing step wedge number versus density were generated using the step wedges at the bottom of each multispectral record. An examination of these curves shown in Figure 1 indicates that the printing exposures, as well as the curve shapes, were well matched. The relatively high minimum density (approximately .4)

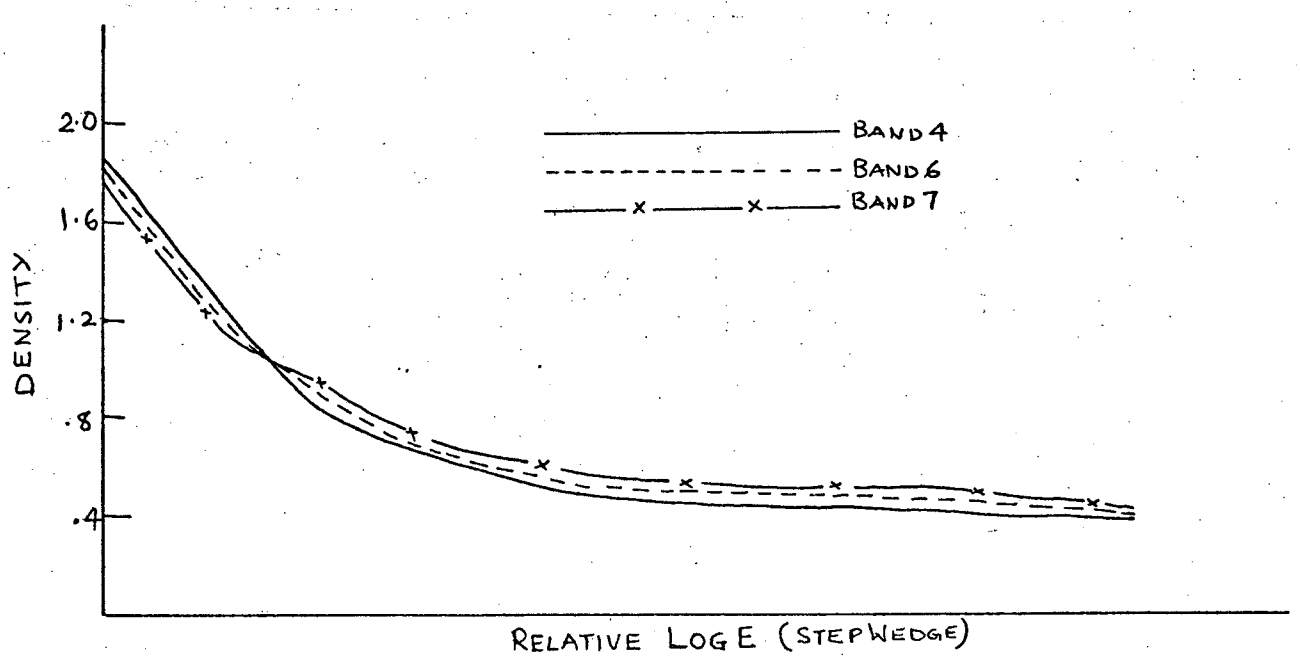

Figure 1. Characteristic curves of ERTS-1 multispectral scanner imagery of the Willcox Playa taken on 27 September 1972.

did not provide sufficient brightness when the additive color analysis, as described subsequently, was performed. It should be also noted that the long toe regions of the step wedge number versus density curves indicate that the positive imagery was exposed and processed for the darker portions of the scene. That is, the density differences are greatest for areas of low brightness, while almost no density differences occur in the high brightness areas.

In order to evaluate the printing and processing of the four multispectral positives, it was necessary to approximate the relative brightness range of the terrain under evaluation. Contact prints of the 70mm multispectral scanner records are shown in Figure 2. Care has been taken to assure that the densities of the step wedges on the prints match those of the release transparencies as closely as possible. Examining the green band (500-600 nm) first, it is apparent that most of the terrain is in

500 - 600 nm Band

600 - 700 nm Band

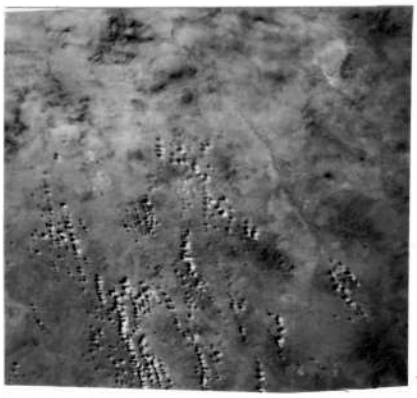

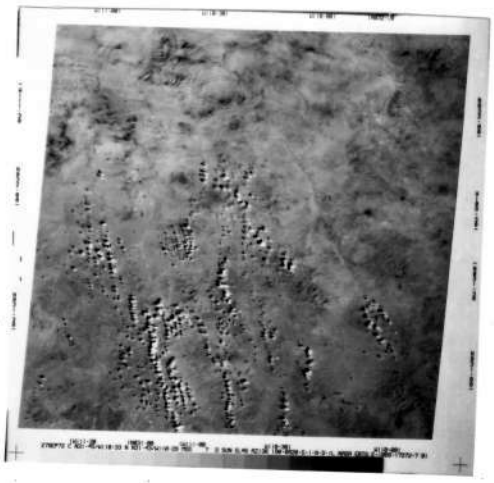

700 - 800 nm Band

800 - 1100 nm Band

Figure 2. ERTS-1 bulk multispectral scanner images taken on 27 September 1972. The Willcox Playa is in the upper right of each photograph.

highlight or, in terms of the step wedge number versus density curve, lies along the toe portion where the density differences are not large. Thus, the imagery appears lacking in contrast, especially in the cultivated land region to the right of the Willcox Playa. The optimization of density differences in the scene, particularly the highlights, could have been accomplished by increasing the exposure of the positive image while maintaining the development parameters constant. The density range of a large portion of the scene lies between the #1 and #8 steps of the gray scale while the mountain ridges have a lower density corresponding to the #13 step. The density differences between most of the terrain objects do not exceed .12; if exposed on the straight line portion of the percent transmission versus density curve, the density differences produced would have been as large as 3.0.

A similar examination of the red band (600-700 nm) shows considerably more detail than was present on the green band. This increase in detail results from an improved contrast between objects in the scene (for example, the cultivated area to the right of the Playa). This increased contrast does not result from any difference in processing, rather it is caused by the fact that the negative material was given sufficient exposure to place the objects of interest more nearly on the straight line portion of the percent transmission versus density curve. The density range of most of the scene lies between steps #9 and #12. The resulting density range is .3.

Both near-infrared positive bands (700-800 nm and 800-1100 nm) have been very poorly exposed, although the contrast is the same as the red band. The high reflectance of the cultivated crops adjacent

to the Playa can barely be differentiated from the barren clay flat of the dry lake bed. This is because both objects, in spite of their inherent brightness differences, lie along the toe of the step wedge number versus density curve. The Playa has an average density of .52, while the crops have a density of .5. These values correspond to steps #8 and #7 on the gray scale. If the printing exposure had been increased, the density differences between these two objects could have been increased from .02 to .4.

The set of NASA released positives shown in Figure 2 were placed into the Spectral Data Model 64 viewer for recombination in additive color. Figure 3 is a photograph of the viewer screen in which the 500-600 nm multispectral scanner band was projected as blue, the 600-700 nm band as green, and the 700-800 nm band as red. This rendition is an approximation of that which would be achieved using color infrared film. Because of the incorrect printing exposure of the positives, the imagery lacks image detail, contrast, and color.

Figure 3. Additive color rendition using NASA bulk positives in which the 500-600 nm (green) band is projected as blue, the 600-700 nm (red) band as green, and the 700-800 nm (near-infrared) band as red.

The second set of ERTS multispectral scanner data analyzed over the Willcox Playa test site was acquired on 14 October 1972. The nadir of these photos is considerably eastward of that taken on September 27th. The relative step wedge number versus density curves shown in Figure 4 were generated using the step wedges along the lower edge of each record.

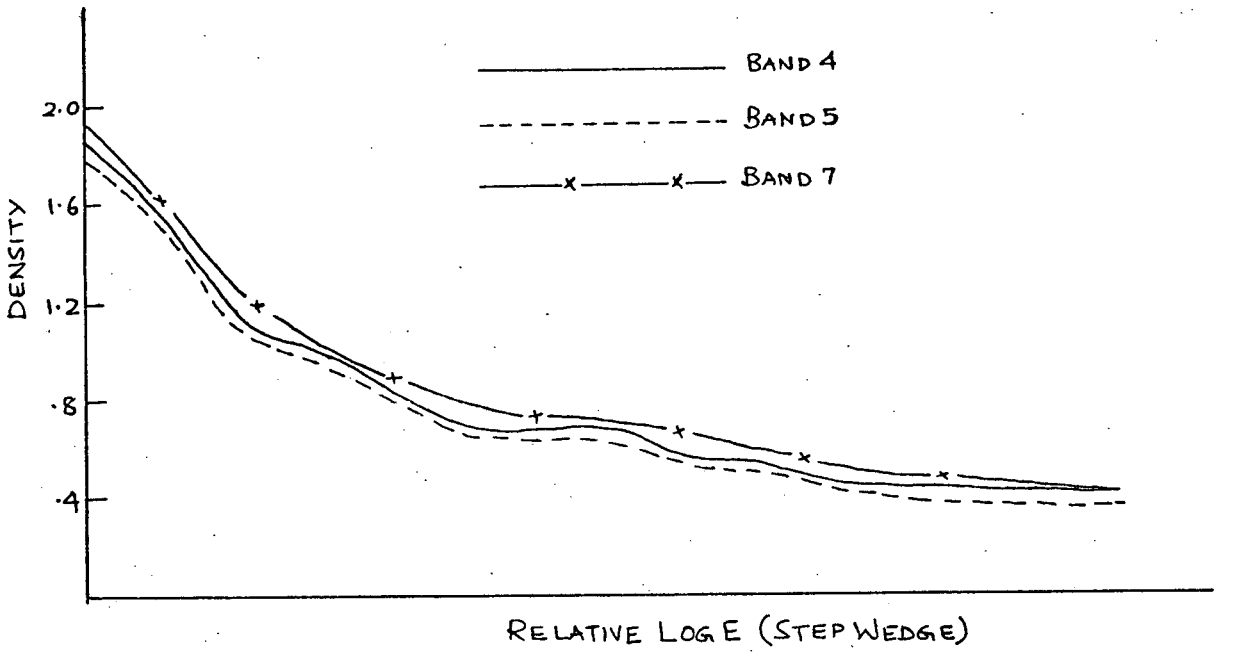

Figure 4. Step wedge number versus density of multispectral scanner bulk positives of area covering the Willcox Playa, Arizona, taken on 14 October 1972.

A comparison of this set of curves with those of Figure 1 shows that there exists a larger scene brightness range which is imaged on the upper portion of Figure 4. In other words, the exposure has been increased. There has also been an increase in the slope of the step wedge number versus density curve for these later multispectral photos which are shown as contact prints in Figure 5. Each of the multispectral scanner positives

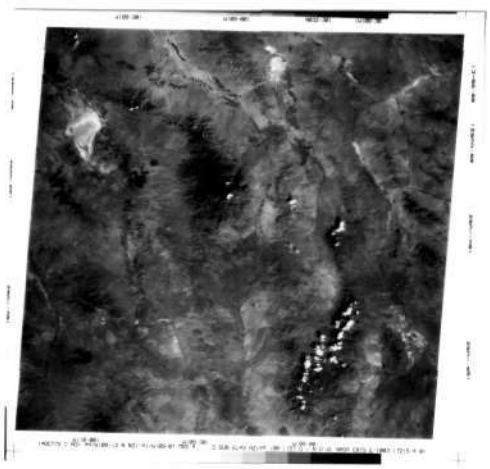

500 - 600 nm Band

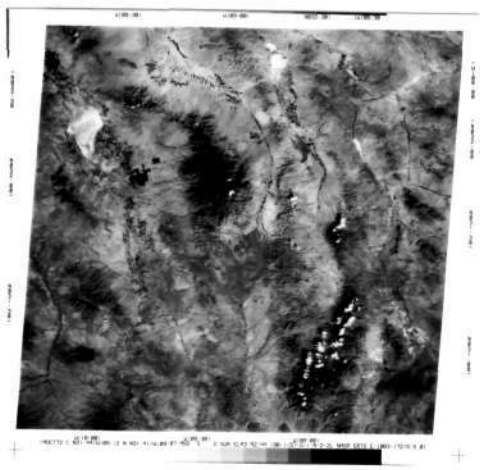

600 - 700 nm Band

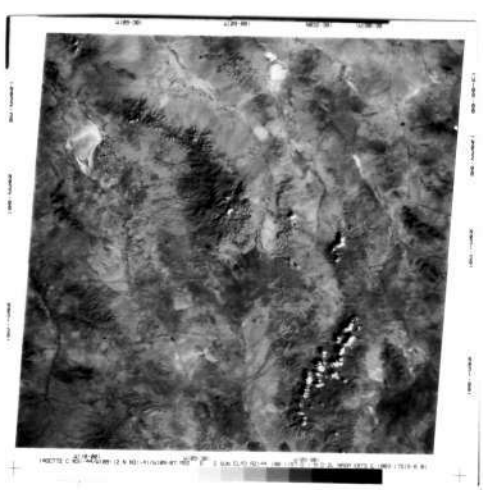

700 - 800 nm Band

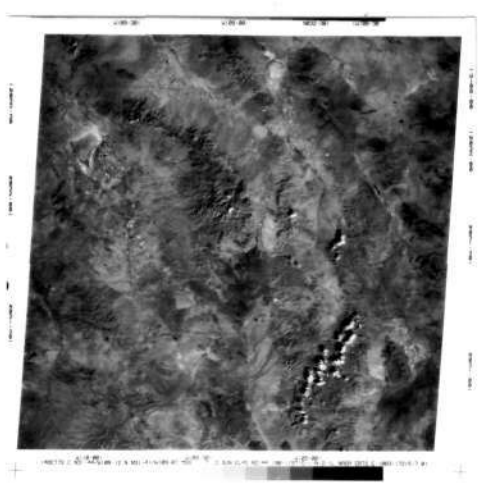

800 - 1100 nm Band

Figure 5. Contact prints of ERTS-1 multispectral scanner bulk images taken on the Willcox Playa, Arizona, on 14 October 1972. The Playa is in the upper left of each photo.

are well matched in curve slope and minimum density.

Comparing the green bands (500-600 nm) of Figures 5 and 2 shows a marked improvement in the image detail for the cultivated land areas to the southeast of the Willcox Playa; this, in spite of the relative increase in density, is a much better positive image for analysis in an additive color viewer.

The black-and-white positive for the red band (600-700 nm) shows that most of the scene lies between steps #6 and #10 on the transmission gray scale located at the bottom of the image. This represents a density difference of only .3. The most dense images in the photo correspond to step #13 which lies just at the start of the straight line portion of the percent transmission versus density curve shown in Figure 4. In other words, a significant portion of the curve is not being utilized at all. The highlight areas of the Willcox Playa are in the fog density level of the film so that the entire scene exists along that part of the curve which yields the least discrimination in terms of density. The base-plus-fog density level for all MSS bands exposed on 14 October is excessively high, being .49.

Figure 6 is a composite additive color image in which the green band (500-600 nm) record was projected as green and the red band (600-700 nm) was projected as red. This rendition is a simulation of a true color photograph exposed through a minus blue haze cutting filter. Notice that the overall image brightness is low because the base-plus-fog densities on both records are extremely high. The color of the image tends to yellow because of the additive combination of red and green light. This

Figure 6. Composite additive color rendition of ERTS-1 imagery of Willcox, Arizona, acquired on 14 October 1972. The 500-600 nm (green) band is imaged as green and the 600-700 nm (red) band is imaged as red.

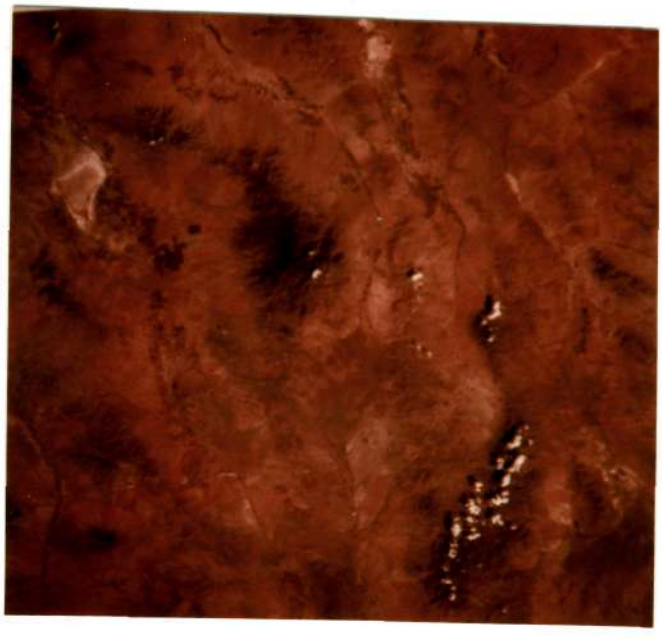

Figure 7. A variation of the additive color rendition shown above in Figure 6 in which the 500-600 nm (green) band has been imaged as cyan (blue-green).

is an unnatural appearance which most photo interpreters find difficult to use. In order to simulate a more realistic true color presentation on the screen, the green projection filter which had been used to project the 500-600 nm band was replaced by a blue-green (cyan) filter. The result is shown in Figure 7. This color presentation has a more natural appearance because of the addition of some blue light for color balancing.

A simulation of color infrared film, shown by Figure 8, was generated by projecting the 500-600 nm (green) band as blue, the 600-700 nm (red) band as green, and both the 700-800 nm and 800-1100 nm infrared bands as red. The brightness of each near-infrared channel was reduced to half value so that when projected their combined brightness would be the same as a single infrared channel projected at full brightness. Figure 9 shows a false color presentation generated by projecting the 500-600 nm green band as red, the 600-700 nm red band as blue, and the 700-800 nm infrared band as green.

The most recent set of scanner data analyzed herein was obtained on 2 November 1972. The nominal nadir of the scanner frame is directly north of the 27 September frame. Contact prints of the four NASA release bulk positives are shown in Figure 10 and the step wedge number versus density curves associated with them are given in Figure 11. The exposure of the positive images, as well as the processing conditions, are almost identical with those of 14 October, except that the minimum density is .1 lower.

The overall density of the 500-600 nm (green) band image lies between the #8 and #12 steps of the positive wedge which represents a density difference of .52. The center of the Playa has an average density of 1.05

Figure 8. Composite additive color rendition of 14 October 1972 ERTS-1 imagery in which the 500-600 nm (green) band is imaged as blue, the 600-700 nm (red) band is green, and both the 700-800 nm and 800-1100 nm infrared bands as red.

Figure 9. Composite additive color image similar to that above in which the 500-600 nm band is imaged as red, the 600-700 nm band is imaged as blue, and only the 700-800 nm infrared band is imaged as green.

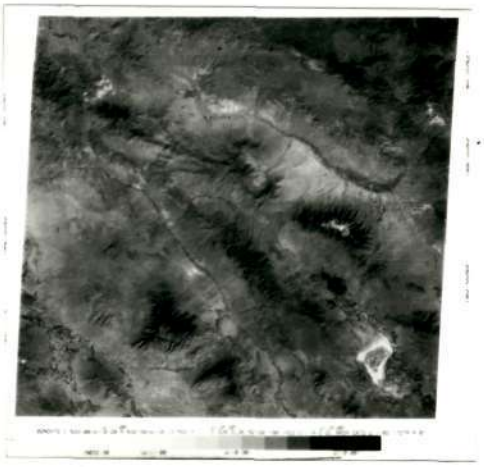

500-600 nm Band

600-700 nm Band

700-800 nm Band

800-1100 nm Band

Figure 10. Contact prints of ERTS-1 multispectral scanner bulk images taken of the Willcox Playa, Arizona, on 2 November 1972. The Playa is in the lower right of the photo.

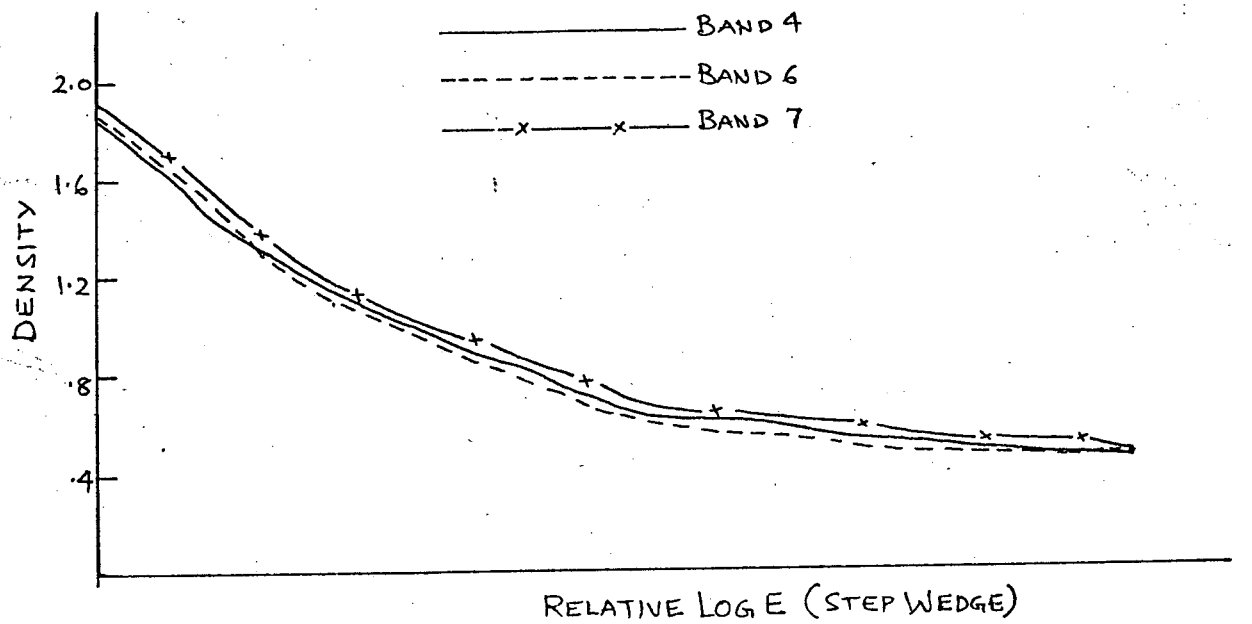

Figure 11. Step wedge number versus density curves of ERTS-1 bulk 70mm positive transparencies of Willcox Playa, Arizona, taken on 2 November 1972.

and shows considerably more contrast within it than either of the previous sets of scanner data. Positive exposure of the green band is heavy and no portion of the scene lies along the straight line of the step wedge number versus density curve. The overall density range of the 600-700 nm (red) image lies between steps #7 and #13 on the positive wedge which represents a density difference of 18. The red image appears to be much "sharper" than the green in terms of inherent contrast, although the overall density ranges do not differ by more than .28. This is due to a color contrast which exists as a result of the spectral reflectance of the terrain.

A color infrared simulation of the 2 November 1972 imagery has been generated by projecting the 500-600 nm (green), 600-700 nm (red), and

700-800 nm near-infrared bands as blue, green, and red respectively in a Spectral Data Model 64 additive color viewer. Figure 12 is a color copy of this rendition created on the viewer screen. The multispectral screen brightness factor is low due to the high base-plus-fog factor. A change in the reflectance of the Playa can be seen by comparing this rendition to Figures 3 and 9.

Figure 12. Additive color rendition of 2 November 1972 ERTS-1 imagery in which the 500-600 nm (green) band is projected as blue, the 600-700 nm (red) band as green, and the 700-800 nm (infrared) band as red.

2.2 Time Sequence Multispectral Color Analysis of ERTS-1 Data

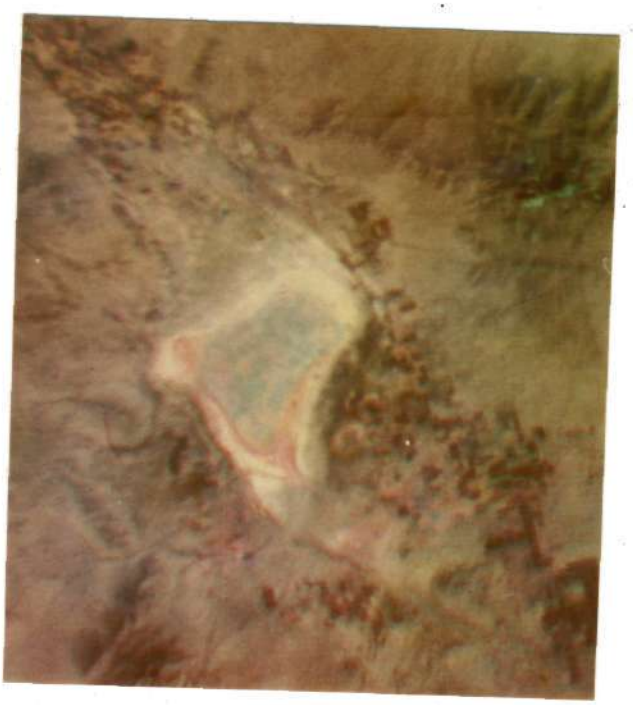

The photo above is a sequential multispectral color reproduction of three ERTS images of the Willcox Playa, Arizona. This type of presentation is useful for detecting changes over time, such as ground surface moisture, by showing them as colors. The original black-and-white multispectral images were acquired on September 27, October 14, and November 2, 1972. All three were taken in the red part of the spectrum (600-700 nm). A color composite of the three was made by reprocessing the original NASA negatives for maximum contrast in the bright playa portion of each of the three images, projecting them in superimposed registry on our additive color viewer, and then making a color photo of the result. The November 2 image was projected as red, the October 14 as green, and the September 27 image as blue.

When interpreting the characteristics of the Willcox Playa in the sequential multispectral color photo on the previous page, the scientist can draw the following conclusions from the colors presented in various portions of the image of the dry lake bed (playa).

-- A colorless shade of white or gray indicates no change in surface moisture content between 27 September and 2 November 1972.
-- Yellow indicates areas where a decrease in soil moisture occurred between 27 September and 14 October and little change from 14 October to 2 November.
-- Orange also indicates a decrease in soil moisture between 27 September and 14 October, coupled with a reduced rate of decrease to 2 November.
-- Cyan or red are areas where moisture changed little between 27 September and 14 October, then increased greatly by 2 November.
-- Red indicates areas where surface water did not change between 27 September and 14 October, then decreased between 14 October and 2 November.
-- Green indicates a reduction in surface moisture from 27 September to 14 October and an increase between 14 October and 2 November.
-- Blue indicates the opposite effect from those areas that yellow; i.e., surface moisture increases between 27 September and 14 October

with no change between 14 October and 2 November.

Figure 14.

The above photo is a close-up typical of the surface of the northwest portion of the Willcox Playa when dry.

2.3 Spectral Reflectance Measurements of the Willcox Playa

Willcox Playa, located in the southeastern part of Arizona, is a large dry lake which is clearly resolved on ERTS-1 imagery. It is bounded on the southeast and northeast by cultivated fields and coarser alluvial slopes to the west. The Playa surface is flat and periodic flooding serves as a leveling agent. Variations in sediment size and composition, as well as the availability of surface and ground water, produce a variety of landforms. The central region of the Playa is hard, compact crust which has no micro-

relief, except that created by mud shrinkage. The dry surface consists of mud polygons which are a light gray buff color. Soft, dry, and porous surfaces are often salt-stained and lead to the sticky-wet areas found where the water table is near the surface. The soft puffy soils are usually a light brown color depending on the salt and moisture content. The Playa is dynamic and it changes in response to the surrounding terrain. The surface drainage on and adjacent to the dry lake changes as a function of the rainfall and a technique is necessary to monitor the dynamics of the area. Spectral reflectance measurements of the dry Playa surface indicate a surprising degree of uniformity.

Prior to the launch of ERTS-1 measurements had been made of the incident solar irradiance spectra at the Willcox Playa, Arizona. Simultaneous spectroradiometric radiance measurements were obtained of the Playa and large plowed and grass fields adjacent thereto. These data were computer processed to provide relative percent directional reflectance data of homogeneous terrain objects large enough to be well resolved on the space imagery.

The quantitative spectral analysis of soils, vegetation, and rocks requires that simultaneous and accurate measurements of incident and reflected radiation be made. Since the spectral energy reflected by an object varies with that which is incident upon it, the spectroradiometric measurements must be made at the same instant of time. The arrangement of the instrumentation used to obtain simultaneous measurements of incident and reflected radiation is shown in the following Figure 15. Two instruments were required to obtain reflected radiance measurements due to photomultiplier sensitivity limitations.

A spectroradiometer using a wedge interference filter system enabling

Figure 15. Arrangement of instruments for measuring the spectral distribution of incident and reflected solar radiation in the 380-1250 nm region of the spectrum.

the spectrum from 380-1250 nm to be continuously scanned was used to measure the spectral distribution of incident solar irradiance. The instrument was equipped with a diffusing screen so that its directional response was proportional to Lambert's cosine law. This technique of measuring incident irradiance was used since solar energy falls upon the earth's surface and is reflected into an entire hemisphere regardless of its original direction of propagation. True cosine response also eliminates the need for precise aiming of the instrument.

Whereas a radiometer measures in units of energy rate intensity such as microwatts per centimeter square, a spectroradiometer measures

in units of energy rate intensity per bandwidth, such as microwatts per centimeter square per nanometer. This latter system of units is most meaningful for measurements of radiation since a graph of the spectral distribution of radiant intensity versus wavelength can be obtained. The area under such a curve can be made numerically and dimensionally equal to energy available in the spectral bands of the ERTS-1 multispectral scanner. The spectroradiometer used was capable of measuring from 0.01 to 1000 microwatts per centimeter square per nanometer. These values correspond roughly to illumination levels of 0.03 to 30,000 foot candles.

The calibration of the spectroradiometer was verified before and after the experiment. A spectral standard lamp, serially numbered and calibrated against the National Bureau of Standards reference, was used. The lamp was of the ribbon filament tungsten type and had a nominal accuracy of plus or minus five percent relative to the NBS standard.

The half bandwidth of the spectroradiometer used to measure the incident illumination is approximately 15 nanometers in the 380-750 nm range and 30 nanometers in the 750-1250 nm range. Stray light response to unwanted wavelengths of 15 nm bandwidth and far from the wavelength of interest is usually in the order of 0.01 percent.

The periodic calibration of the spectroradiometer used for measuring incident sunlight allowed an accuracy of plus or minus seven percent in the long wavelengths and plus or minus ten percent in the short wavelengths of the spectrum. Most of this error, of course, comes from uncertainty in the secondary standard used. The relative accuracy of all points with respect to each other throughout the wavelength range measured is approximately plus or minus three percent.

The reflectance radiometer system allowed measurements of the average power of the solar radiation reflected by soils and vegetation in the Willcox Playa area. By means of a grating monochromator, these readings can be made at selected wavelengths over a bandwidth determined by the grating and slits. This instrument basically consists of an optical system which limits the entrance of energy to a twelve degree field, a monochromator grating to spectrally isolate the visible energy to a five nanometer halfband pass, and the infrared energy to a ten nanometer halfband, as well as detector heads to sense the magnitude of the incident energy.

The reflectance spectroradiometer is designed so that light reflected from an object passes through a diffuser system and is directed by the collective lens into the monochromator housing via the entrance slit. Calibration accuracy is obtained when the light incident on the diffuser is imaged on the entrance slit, completely filling the slit area with light. A collective lens in the beam input optics in front of the monochromator entrance slit, collects the incident light which is properly matched with the diffuser to create a uniform illuminating bundle inside the monochromator housing. This bundle of light is then incident on a plane diffraction grating where it is angularly dispersed according to wavelength. Each wavelength present in the source bundle reflects off the diffraction grating at a different angle. The grating can be rotated to direct any selected wavelength bundle onto the center of a concave mirror. The mirror collects the light and, with the help of a quartz corrector lens, forms an image of the entrance slit on the exit slit.

The visible range grating is a 1350 groove per millimeter grating

covering from 350-800 nanometers in the first order and is blazed at 500 nanometers. The reciprocal linear dispersion is 6.4 nanometers per millimeter. The combination of grating and slits determines the dispersion of the system. The effective widths of the visible grating was 20 nanometers as determined by the entrance and exit slit widths are 2.68 and 1.5 millimeters respectively. These particular grating widths were selected in order to obtain sufficient photomultiplier response when measuring targets of low reflected brightness.

The visible spectroradiometer utilized a photo diode detector to produce a signal proportional to the intensity of the light which strikes it. However, in order to obtain sufficient sensitivity in the infrared, a cooled photomultiplier detector must be used to produce an output signal which is of sufficient amplitude to allow significant results to be obtained.

Readout was accomplished using a self-ranging picoammeter. This device has the advantage of displaying digitally the detector current output of the spectroradiometers. Thus calibration and dark current values can be readily obtained and monitored. In addition, no scale switching is required and readings can be obtained rapidly.

In order to obtain accurate data, the spectroradiometers were calibrated before and after the experiment. The calibration of the instrument can shift due to such factors as the collection of dust on the optical surfaces or a variety of other random factors. The electronic circuitry of the instrument is very stable and maintains uniform response but, nevertheless, the accuracy of the instrument was verified.

Data Analysis Techniques.

If a sufficient number of sets of independent measurements of incident and reflected radiation (at 27 points in the spectrum from 350-1100 nm) are made and the readings averaged at each wavelength, it is possible to make the Central Limit Theorem apply to the distribution of average reflectance values. Thus,

$$z_{ij} \equiv \left[\frac{x_{ij1}}{y_{ij1}} + \frac{x_{ij2}}{y_{ij2}} + \frac{x_{ij3}}{y_{ij3}} \right] \frac{100}{n}$$

where: $x_{ijk} \equiv$ the k th measurement of reflected radiation at wavelength i, object j.

$y_{ijk} \equiv$ the k th measurement of incident solar radiation at wavelength i, object j.

$z_{ij} \equiv$ the average percent directional reflectance at wavelength i, object j.

$n \equiv$ number of readings.

By the Central Limit Theorem, the distribution of z_{ij} will be approximately normal regardless of the distribution of the individual values of x_{ijk} and y_{ijk}. This, of course, assumes that measurement errors are independent and randomly distributed.

At each wavelength, for each object, the density spectra is also computed:

$$d_{ij} = \log \frac{100}{z_{ij}}$$

The power which would be reflected if the object had incident upon it radiation emitted by a standard sun is also calculated as follows:

DATE:3/6/69
TIME:1140-1210 MST
WEATHER + LOCATION:CLR. WILL ARI
TARGET:GRASS

WAVE LENGTH (NM)		SUN READING (UW)	ACT. SUN SPECTRA (UW)	REFLECT READING (W*E-10)	ACT. REF SPECTRA (UW*E-2)	PERCENT DIR. REF. (E-1)	DENSITY SPECTRA	STD. SUN REFLECT (UW)
380		15.5	72.912	1.633	6.225	.853768	3.06866	1.40872
400		66	105.336	3.69	11.929	1.13247	2.94597	9.51278
425		127	131.699	6.27	19.1724	1.45577	2.8369	21.8366
450		179	151.255	10.41	27.0316	1.78716	2.74783	37.5303
475		205	160.105	12.08	30.4029	1.89894	2.72149	44.625
500		204	153	13.3	30.7696	2.01108	2.69657	48.266
525		195	139.815	21.7	47.2322	3.37819	2.47131	79.3876
550		160	133.92	23.1	57.1494	4.26743	2.36933	85.3436
575		160	132	16.89	47.5724	3.60397	2.44322	72.0794
600		178	124.778	12.2	40.4064	3.23826	2.48969	72.3609
625		169	117.793	7.88	33.6515	2.85684	2.54411	51.422
650		167	111.222	4.43	27.715	2.49186	2.60347	52.3291
675		176	113.344	2.09	22.3045	1.96786	2.706	44.2763
700		145	97.73	1.677	35.5271	3.63523	2.43947	67.2517
725		147	88.641	1.648	77.3462	8.72579	2.05919	161.427
750		125	81.75	.917	115.791	14.1641	1.84831	226.625
750	*	93	88.9735	5145.46	119.481	13.4841	1.87073	167.09
750		61	96.197	10290.	123.171	12.8041	1.89265	107.554
800		58	79.228	12650.	121.946	15.3918	1.81271	123.134
850		53	71.338	12670.	111.876	15.6825	1.80458	109.778
900		44	58.872	9490.	81.7089	13.8791	1.85764	77.7223
950		32	41.824	4550.	47.6385	11.3982	1.94347	43.2829
1000		36.5	45.8075	3230.	55.879	12.1987	1.91369	59.7734
1050		34.5	39.675	1150.	54.2915	13.6841	1.86378	64.3151
1100		30	29.91	218.	42.51	14.2126	1.84732	55.4293
1150		16.5	15.9225	28.8	24.9955	15.6982	1.80415	29.0417
1200		19	15.435	10.7	34.4487	22.2465	1.65274	36.7067

* = AVERAGE OF TWO INSTRUMENT READINGS

Figure 16. Typical computer printout of spectral measurements showing percent directional reflectance (6th column) at each wavelength (1st column).

$s_{ij} = z_{ij}$ X (standard value for each i)

Both d_{ij} and s_{ij} have been developed to estimate the density of the image on multispectral photography. These estimates are currently in the process of refinement and are auxiliary to the spectral analysis which is contained herein.

A flow diagram of this computer program is shown in the figure below.

Note: Computed for (1) each wavelength
(2) each object

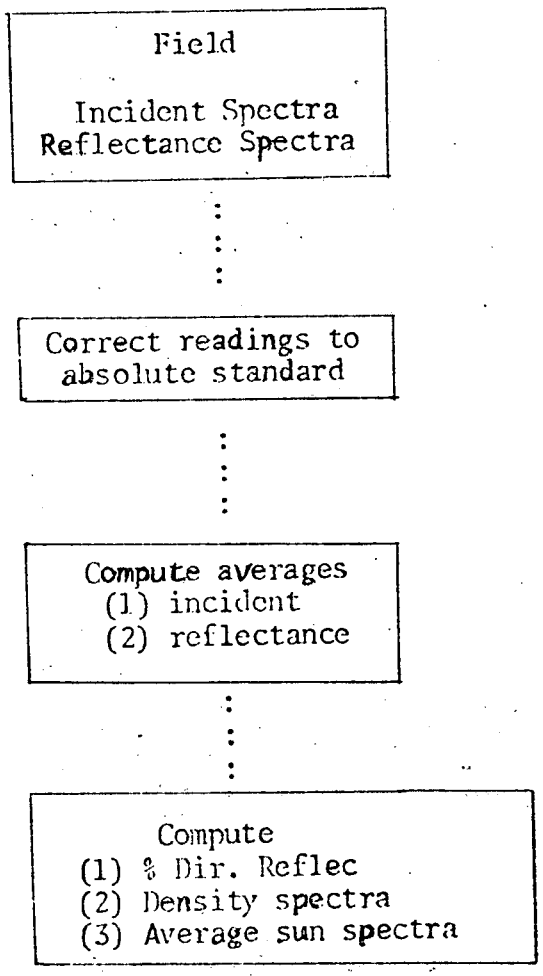

Figure 17. Flow diagram of percent directional reflectance readings.

Computer Output:

The computer output format of the computations performed on the incidence and reflectance spectra is shown in Figure 16. Associated with each wavelength (first column) is the instrument reading (second column) and corrected value of incident sunlight (third column) in microwatts per square centimeter. The reflectance measurements and associated corrected readings (which are determined by the standard lamp calibration) are shown in the fourth and fifth columns.

The percent directional reflectance value shown in the sixth column is the ratio of the value in the fifth column divided by that in the third column. The last column is the value of a standard illuminant times the percent reflectance. Thus, the actual power reflected by an object can be computed by knowing the incident radiation and the data in the sixth column of this output.

Figure 18 shows the associated computer plot of percent directional reflectance as a function of wavelength. This is an example of the percent directional reflectance of grass obtained in situ. The chlorophyll reflection band at 550 nm and chlorophyll absorption band at 675 nm are clearly evident as is the mesophyll reflection above 725 nm.

Incident Solar Radiation:

The intensity and spectral distribution of solar radiation falling upon the earth's surface varies with solar angle and atmospheric conditions. Measurement of the absolute amount of solar energy which strikes the terrain is important since all ground objects reflect different amounts of radiation in each spectral band which is in direct proportion to that which is incident.

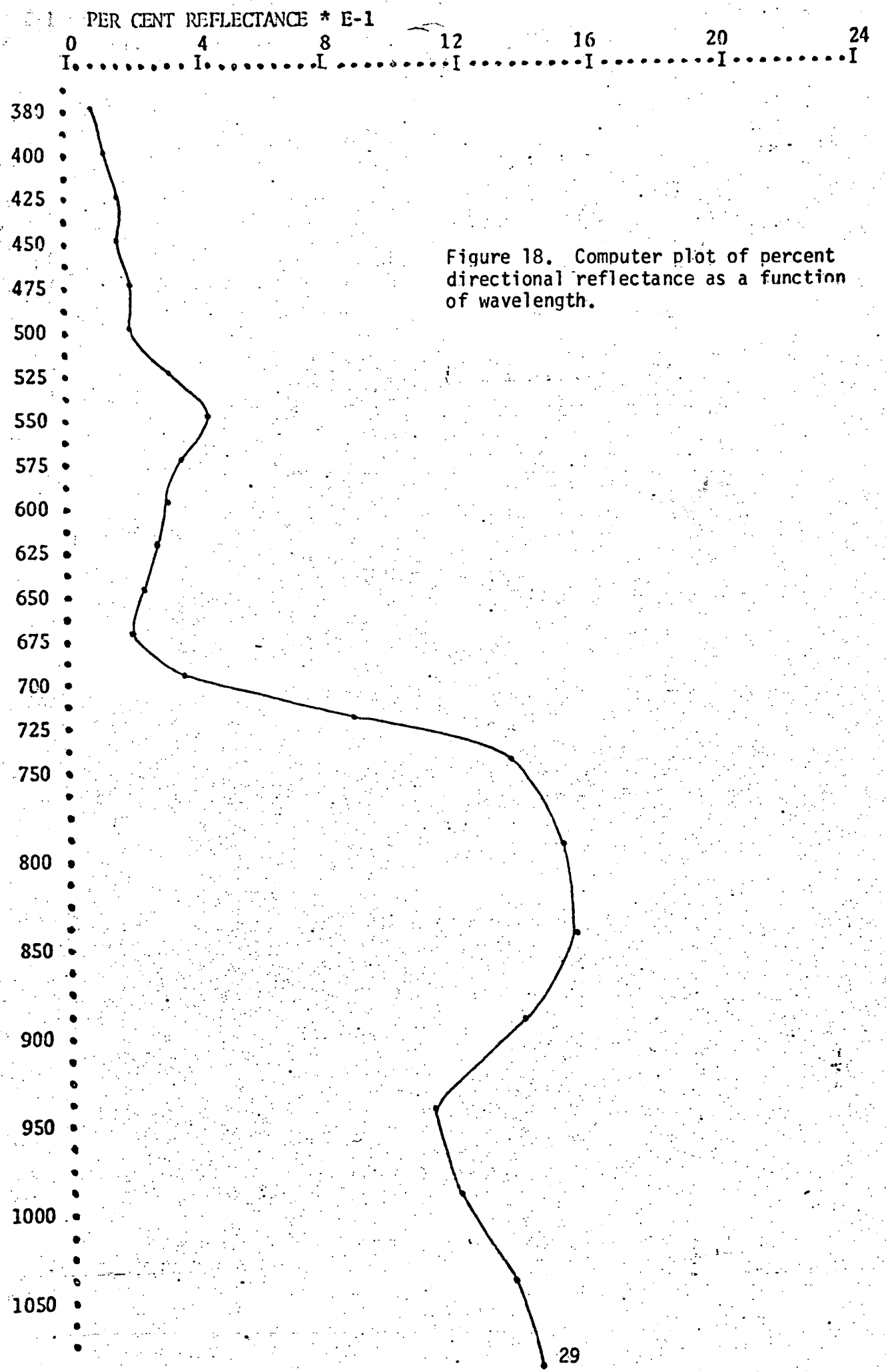

Figure 18. Computer plot of percent directional reflectance as a function of wavelength.

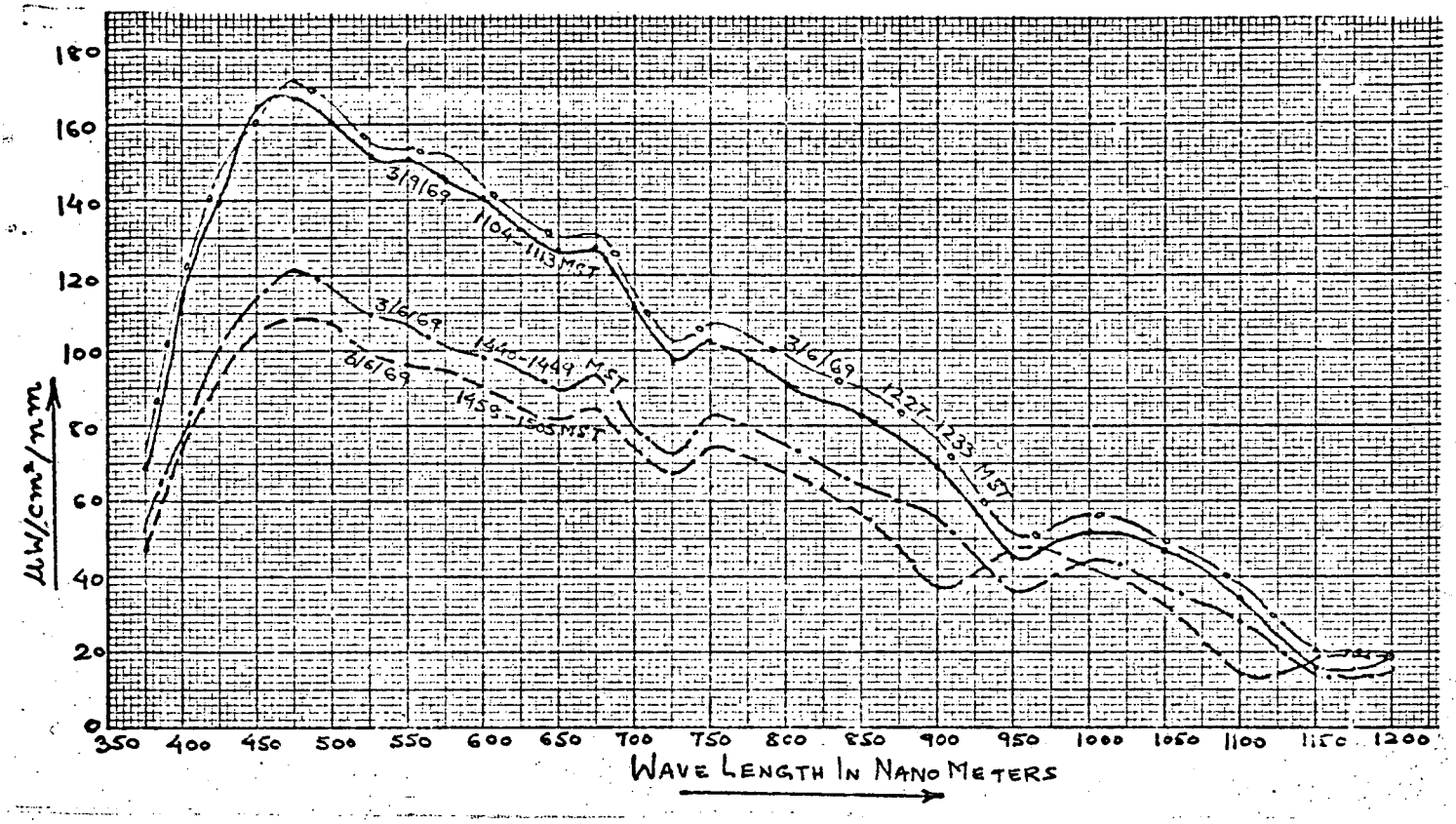

Figure 19. Spectral distribution of solar radiation incident at the Willcox Playa test site at different times during the day.

Theoretical analysis of solar illumination based upon air mass calculations and Raleigh scattering are of little practical value in predicting the spectral distribution of solar energy which actually reaches the ground. This is primarily due to the existence of unknown amounts of Mie scattering and absorption in the atmosphere due to particles which are large compared to the wavelength of the radiation.

Figure 19 demonstrates this condition. Spectroradiometric readings of solar energy (both sunlight and diffuse skylight) using a lambertian detector were measured during a four day interval at Willcox, Arizona. Spectral intensity in microwatts per centimeter squared per nanometer from

380-1200 nanometers is shown for four of these measurements between 1104 and 1515 MST.

The first feature clearly evident from this data is the large variation in intensity with wavelength as a function of time (solar angle). The characteristic absorption band below 380 nanometers at 725 and 950 nanometers is also clearly evident.

The percent directional reflectance of the Willcox Playa, Arizona, was obtained for two adjacent areas at the location shown in Figure 20. Simultaneous spectroradiometric measurements of incident global solar radiation were made along with measurements of the radiation reflected by the Playa.

The reflectance spectroradiometers were oriented so as to prevent any specular reflection from the Playa surface from entering the input optics of the instrument. The partly cloudy atmospheric conditions that existed required that extreme care and patience be used in making these measurements. The incident and reflected spectroradiometric data were corrected and the percent directional reflectance calculated using the computer program discussed previously.

The percent directional reflectance data presented in Figure 21 indicated a surprising degree of uniformity in the reflectivity of the Playa surface. Although there appears to be slight brightness differences between the two areas, the shape of the reflectance curves is quite similar.

A comparison of the spectra of plowed fields and grass with the Playa is shown in Figure 22. The area from which these readings were obtained was adjacent to the target array at the locations shown in

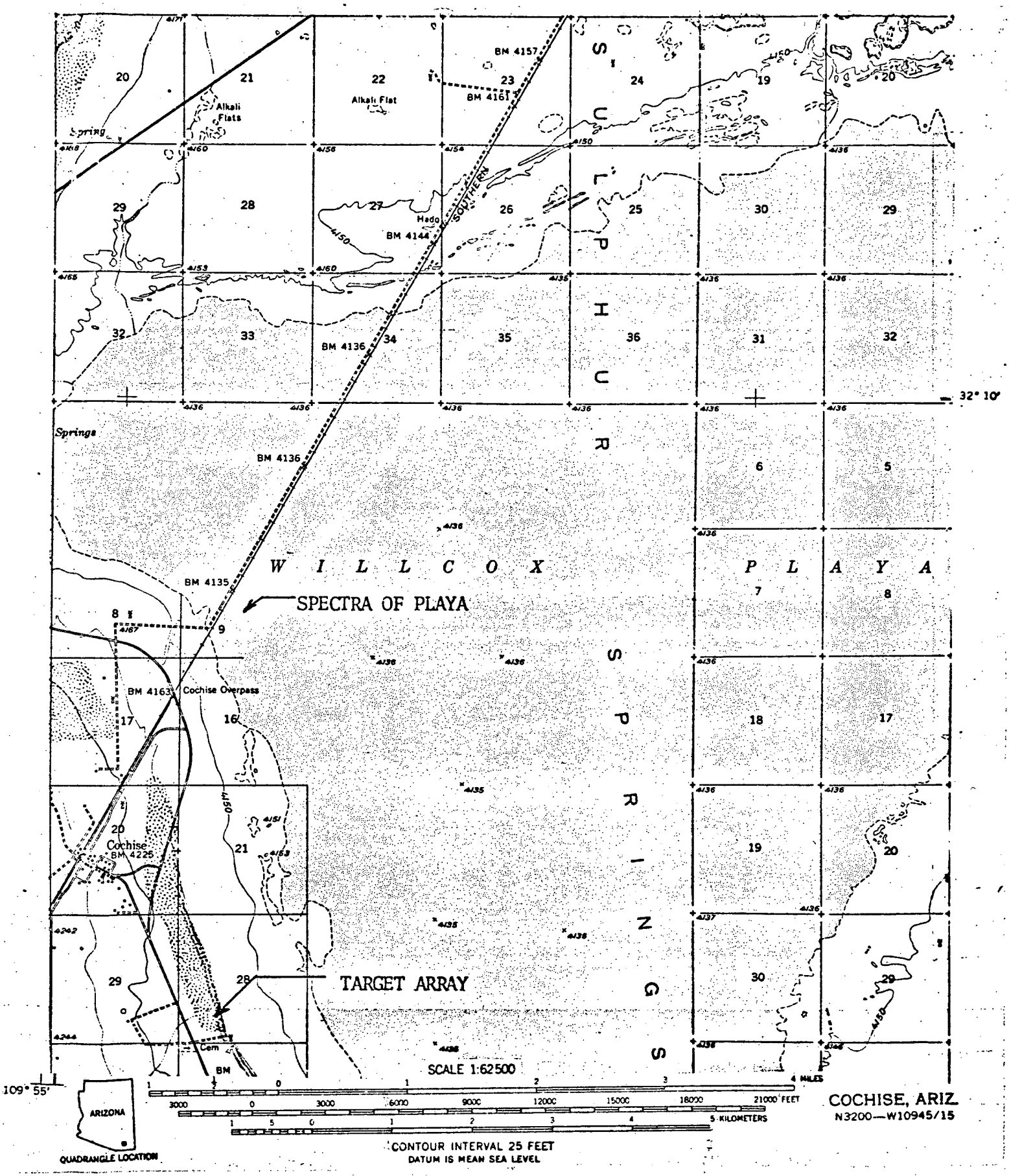

Figure 20. Location at which incident and reflectance spectra were measured.

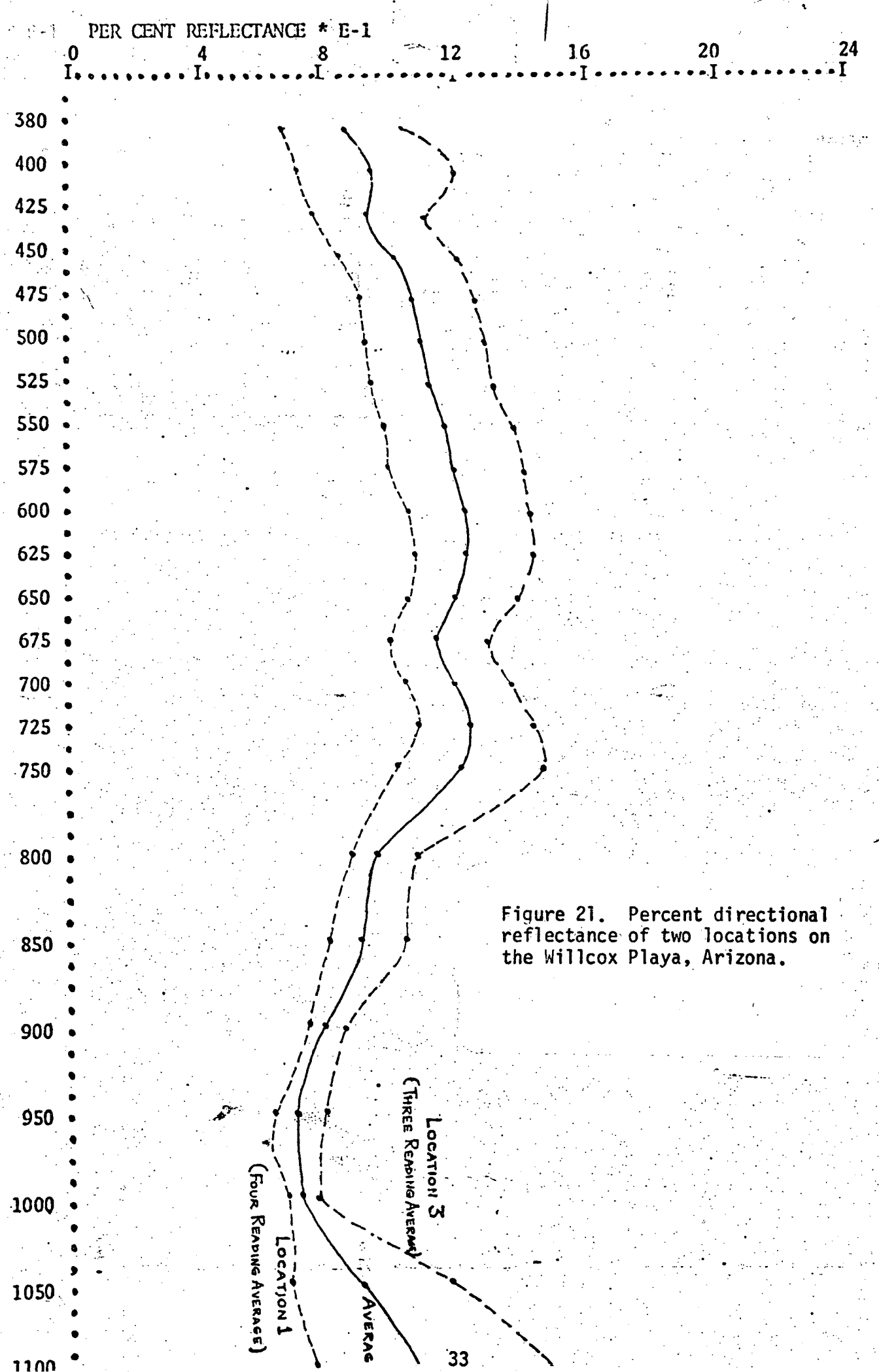

Figure 21. Percent directional reflectance of two locations on the Willcox Playa, Arizona.

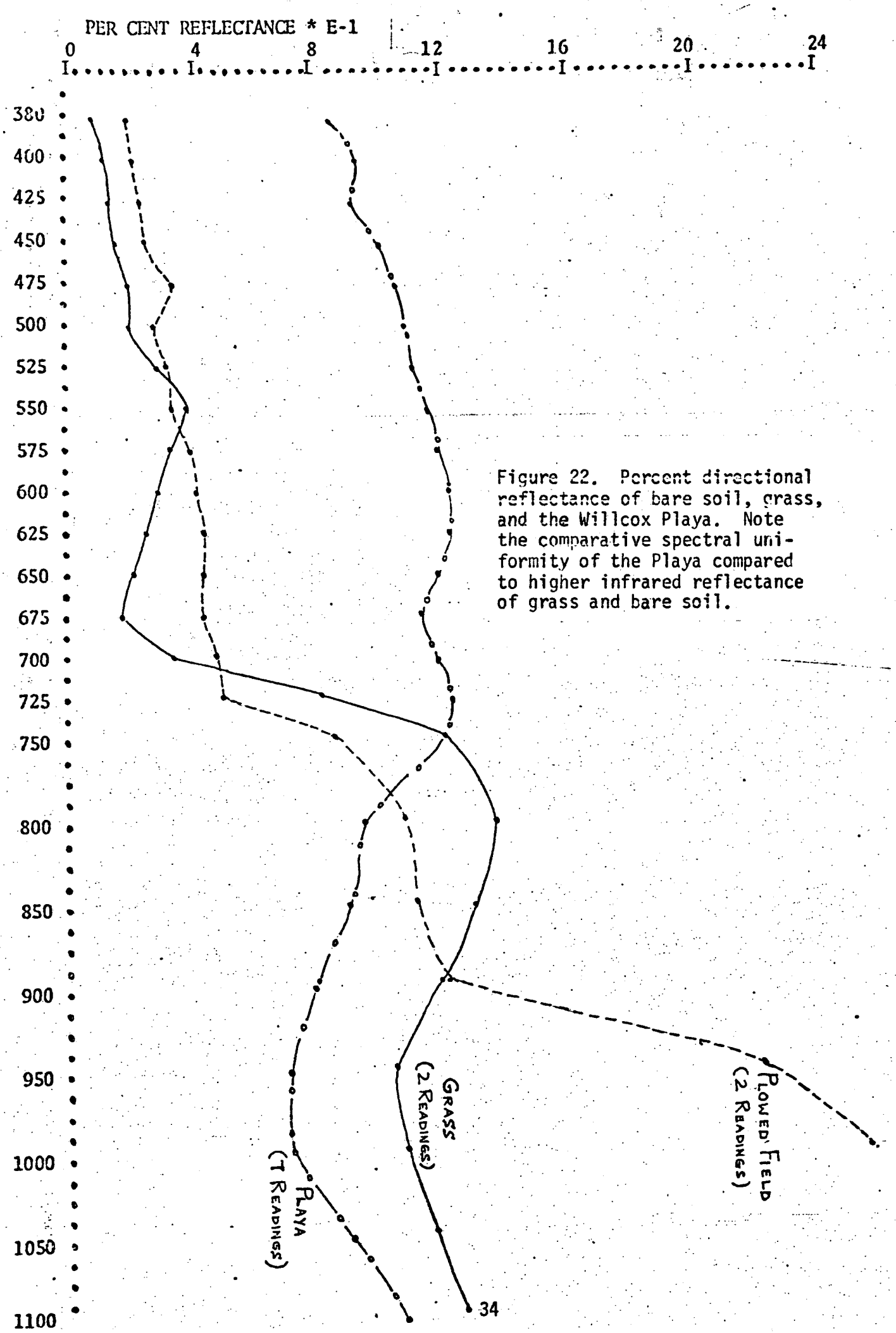

Figure 22. Percent directional reflectance of bare soil, grass, and the Willcox Playa. Note the comparative spectral uniformity of the Playa compared to higher infrared reflectance of grass and bare soil.

in Figure 20. The characteristic chlorophyll absorption band (675 nm), chlorophyll reflection band (550 nm), and mesophyll reflection band (above 700 nm) are shown in the spectra of the grass.

2.4 Reflectance Spectra of Predominant Vegetation in the Prescott National Forest

In situ spectral reflectance measurements were taken of three prevalent vegetation types in the Prescott National Forest. These species are Pinion Pine, Juniper, and Manzanita. Typical reflectance spectra are shown in Figure 23.

Reflectance spectra in Figure 23 were obtained between 23 October and 28 October 1972.

A computerized telespectroradiometer was utilized to collect the in situ reflectance spectra. This truck-mounted instrument is positioned adjacent to the target to be measured (e.g., a Pinion Pine) and the detector head extended in the air to obtain the similar downward perspective as the ERTS multispectral scanner. The instrument measures and stores in the computer memory the reflectance of a standard white plate which is placed in the field of view of the spectroradiometer. The reference plate is then removed and the spectra of the target is obtained. The computer enters all the necessary instrument corrections, divides the standard white plate reference readings into the target readings at each discrete wavelength measured and prints out the result on a teletypewriter. Figure 24 shows this truck-mounted instrument in operation at the Prescott test site.

The detector head mounted atop the extended ladder is comprised of an imagery optical system, a circular interference filter monochromator,

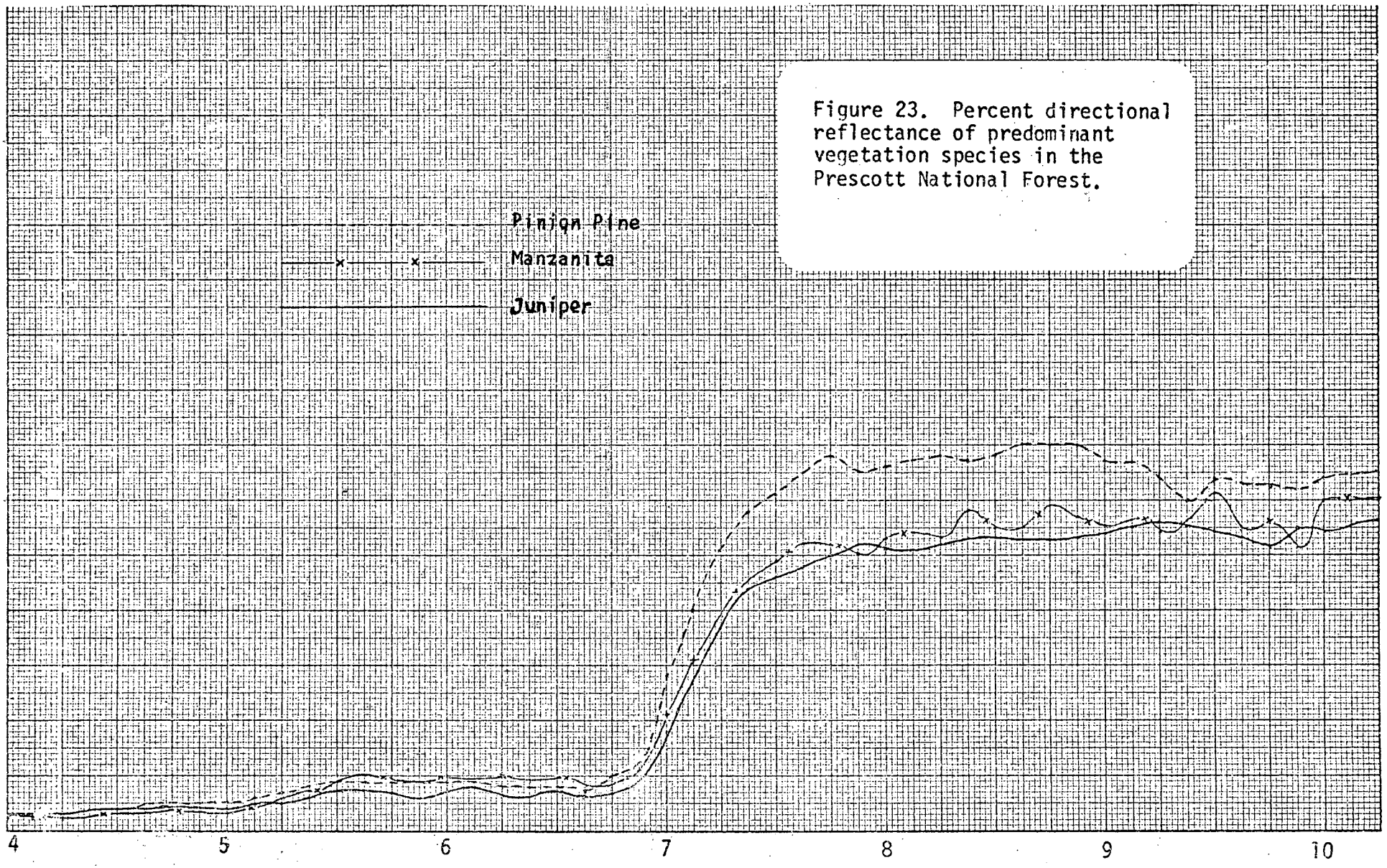

Figure 23. Percent directional reflectance of predominant vegetation species in the Prescott National Forest.

Figure 24. Truck-mounted telespectroradiometer.

visible and infrared photomultiplier detectors, and an electronic amplifier. The circular filter is indexed into position in the optical system in front of the detector which selects the particular wavelength to be measured. Usually 80 discrete wavelengths are measured between 400 nm and 1100 nm.

The ratio of target reflectivity to standard reflectance reference is automatically calculated by the instrument and displayed under computer control. The computer is programmed with a list of spectral ranges (visible and infrared), data points (discrete wavelengths of interest), and the number of scans per data point. The computer incorporated in the spectroradiometer is a 16-bit word length general purpose computer having a 4096 work (8K byte) memory. Four hardware accumulators are used in addition to

a PC register. The basic control program resides in 3000 core locations and includes a floating point interpretive package. The 1000 remaining locations are used for temporary data storage during target data acquisition. The basic control program takes radiometric measurements at pre-determined wavelengths, stored in a look-up table. For reflectance measurements a white standard reflector is compared to the target and the relative reflectance of the target is computed as a ratio of the target to the standard. The computer then uses this responsivity data to calculate the radiance of a target.

The telespectroradiometer used to collect the data contains two spectral channels - one covering from 400 to 700 nm (visible), the other from 675 to 1350 nm (infrared). The system is comprised of an optical head which contains the telescope optics, a sensing head containing the photomultiplier detectors, and input-output control console which contains the computer, motor drives, analog-to-digital converter, and teletypewriter.

The system is designed to have flexibility in the spectral region of operation and in its mode of operation. The primary filter assembly of the system utilizes a circular variable interference filter which allows continuous variance of the spectral region transmitted to the detector as a function of the angular position of the filter. The spectral response typically covers a two-octave range of wavelengths with an average spectral resolution of 2 1/2%. The system operates in an incrementally stepped mode which provides the ability to take precise measurements at each wavelength. Time is allowed for gain ranging, amplifier settling, and multiple readings for computer averaging.

The automatic telespectroradiometer used to collect the data consists

of four basic units: the optical head, the sensing head, the control cabinet, and the output unit.

The telespectroradiometer contains a 300mm focal length refractive optical system with a 50mm diameter entrance aperture. The mechanical configuration of the optical head of the system is shown in Figure 25. The incoming radiation is focused by the objective lens on an intermediate focal plane where an adjustable field stop is located to define the system's field of view.

The radiation passing through the field stop is refocused by the transfer optics onto the front surface of the circular variable filter. The radiation traversing the filter is refocused by a relay lens onto the detector.

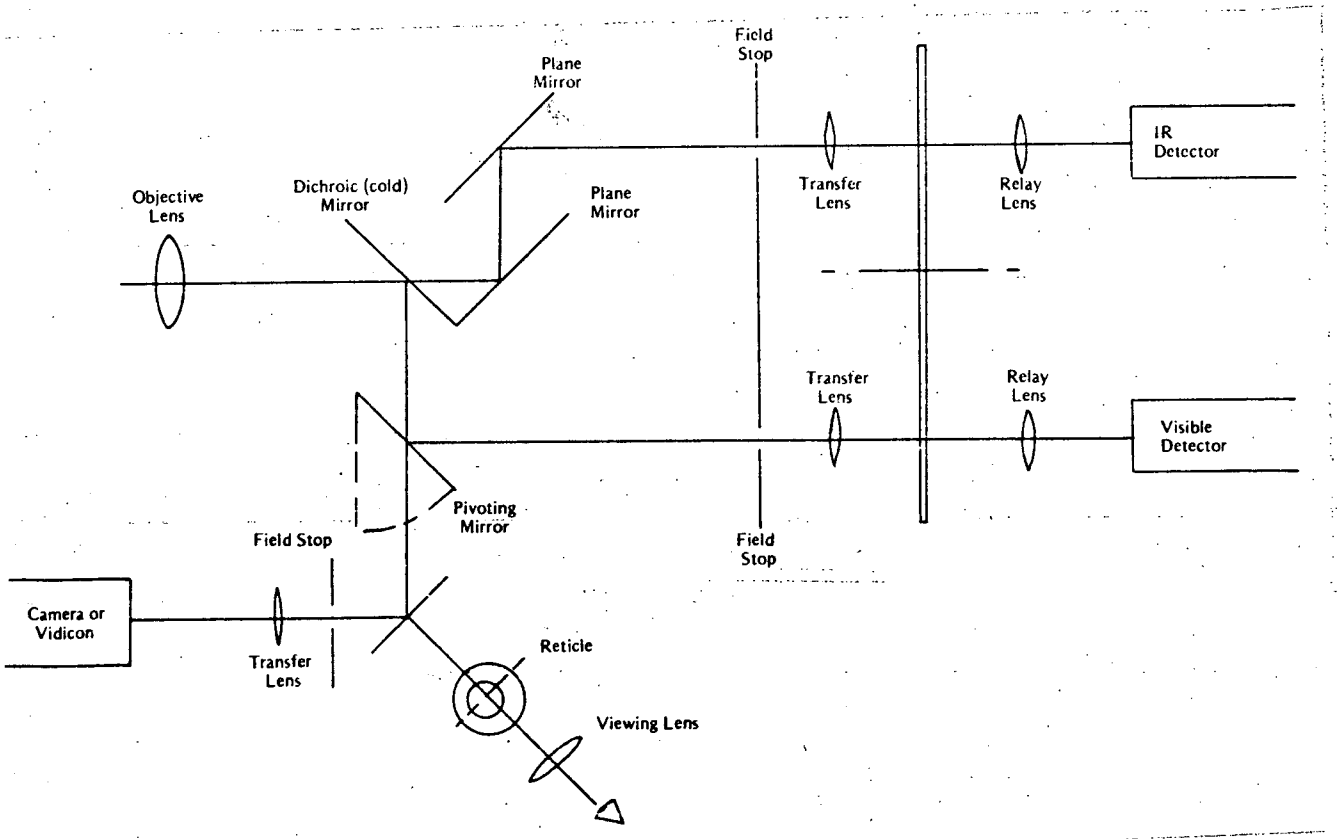

Figure 25. Telespectroradiometer optical schematic.

The circular variable filter is motor-driven under computer control. The direct coupled angular encoder provides a feedback signal to the computer of the instantaneous position of the circular variable filter. The computer program specifies the angular position at which measurements will be made and monitors the optical encoder output until the correct angular orientation is achieved.

The electrical signals generated by the detector(s) are amplified by a picoammeter amplifier with remote gain-ranging controlled by the computer program. The high-level, low-impedance analog output of the amplifier may be transmitted up to a distance of 250 feet to the computer, allowing completely remote operation. Also located in the optics package are the shutter and viewing mirror solenoids, optical encoder buffer amplifiers, and line drivers.

The picoammeter is a two-stage, solid-state amplifier using compact metal-film feedback resistors and solid-state switching for range selection. The program-controlled or manually-controlled shutter allows dark current measurement and corrections to be made under program control without operator intervention. A block diagram of the electronic circuitry is given in Figure 26.

The analog signal from the optical detector is fed to the analog multiplexer of the analog-to-digital input channel. The multiplexer selects the picoammeter output for conversion or other accessory functions, such as internal self-check functions. The multiplexer output drives the sample-and-hold and the eleven-bit analog-to-digital converter. The multiplexer, sample-and-hold and analog-to-digital converter are controlled by the MADC interface which also contains the picoammeter gain control

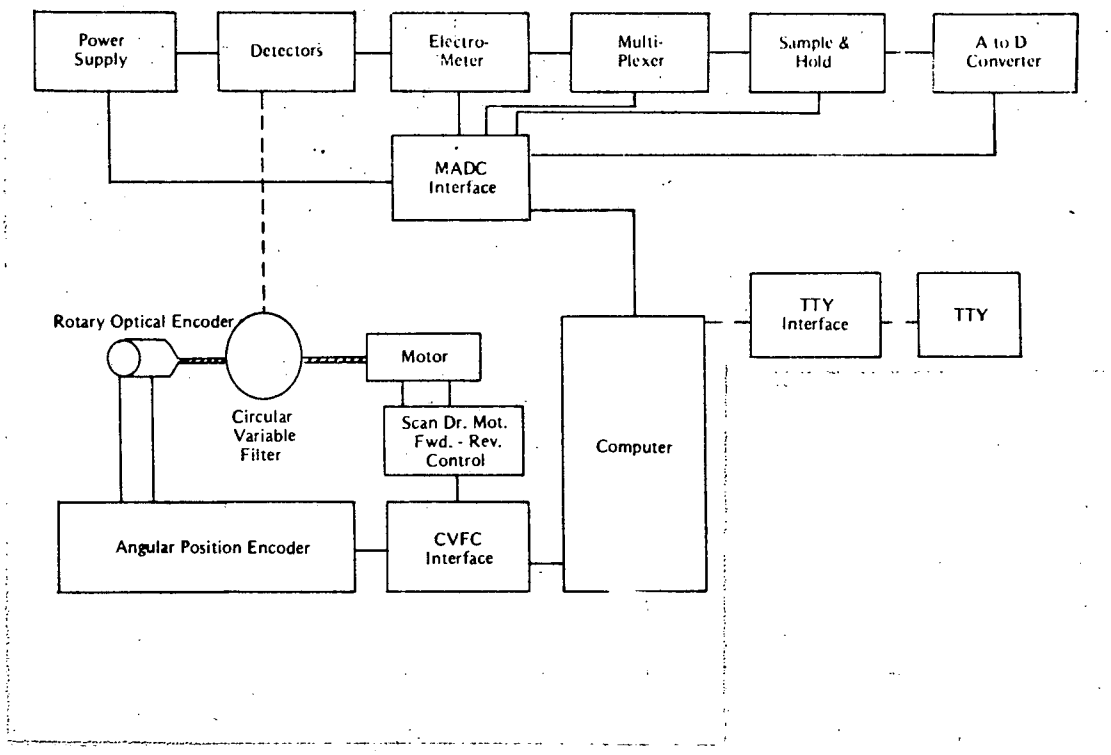

Figure 26. Telespectroradiometer electronics block diagram.

registers, shutter and viewing mirror solenoid buffer registers.

The encoder outputs drive the decoder module which, in turn, drives the present position register in the CVFC interface. The present position register supplies the computer program with the current angular rotational position of the circular interference filter. The CVFC interface contains auxiliary buffer registers for operating the motor drives and synchronization control modules.

Section 3

New Technology

The research reported herein reports the additive color analysis of ERTS-1 imagery and the collection of associated reflectance spectra. Innovations incorporated the use of multispectral imagery taken at different times to create an additive color display showing changes in spectral reflectance in a single spectral band with time.

The technical description of the techniques used to create the additive color display has been given in Section 2.2 of this report.

Section 4

Program for Next Reporting Interval

During the next reporting interval in situ spectral reflectance measurements will be taken of the Willcox Playa, Arizona, simultaneously with the scheduled ERTS-1 data acquisition. Soil moisture data and associated soil samples will be collected and analyzed. These soil data will be correlated with the spectral reflectance and with the ERTS-1 image characteristics of the Willcox Playa.

Quantitative colorimetric measurements will be made of both color composites of ERTS-1 multispectral imagery using the four spectral bands acquired at the same time and of different spectral bands at different times. These image data will be correlated with the ground spectral reflectance and moisture data. Imagery qcquired over Prescott National Forest, Arizona, will also be analyzed and correlated with spectra which have been collected.

Section 5

Conclusions

ERTS-1 bulk multispectral scanner imagery, when recombined in a single additive color presentation, show color differences which are related to spectral reflectance changes of desert dry lakes (Playas). When the same bands acquired at different times are reconstituted in color; changes in reflectance at the same wavelengths with time are shown as colors. In both the above additive color presentations, soil moisture is the probable cause of color to the signatures which have been observed.

The spectral fidelity of ERTS-1 bulk imagery is sufficient to allow such color signatures without requiring photographic reprocessing. Furthermore, the spatial accuracy of the 70mm photographic positives which is disseminated is sufficient to permit good image superimposition of imagery acquired during different 18-day cycles.

Section 6

Recommendations for Further Action

The correct inferences which can be made regarding the spectral reflectance of ground objects using ERTS-1 imagery depend on the accuracy and precision of the exposure versus density relationships contained in the photographs which are disseminated by NASA. If the accuracy of density of each step on the gray scale contained in the lower portion of the ERTS format were established and precision with which each density step was reproduced for each 18-day cycle, it is considered that great improvement in the detection of subtle reflectance of ground objects over time would result.